International Journal of Medical and Pharmaceutical Research

Online ISSN-2958-3683 | Print ISSN-2958-3675
Frequency: Bi-Monthly
Available online on: https://ijmpr.in/

Original Article

Beyond Biopsy: A Synergistic Approach To Brain Tumor Characterization Using Diffusion-Weighted Mri And Proton Mr Spectroscopy

Dr. Bhumika Luniwal[1], Dr. Neeshnat N. Gabhane[2], Dr. Bhavya Chaudhary[3], Dr. Hemant Kumar Mishra[4]

[1]M.D. Final Year Resident, Department of Radio-Diagnosis - Mahatma Gandhi Medical College and Hospital, Jaipur, Rajasthan
[2]D.M. Second Year Resident, Department of Interventional Radiology - Mahatma Gandhi Medical College and Hospital, Jaipur, Rajasthan
[3]M.D. Final Year Resident, Department of Radio-Diagnosis - Mahatma Gandhi Medical College and Hospital, Jaipur, Rajasthan
[4]Professor and Head of Department of Interventional Radiology - Mahatma Gandhi Medical College and Hospital, Jaipur, Rajasthan

Corresponding Author:

Dr. Neeshnat N. Gabhane
D.M. Second Year Resident, Department of Interventional Radiology - Mahatma Gandhi Medical College and Hospital, Jaipur, Rajasthan

Received: 25-10-2025
Accepted: 17-11-2025
Available online: 28-11-2025

ABSTRACT

Background: Non-invasive differentiation of benign and malignant brain tumors remains a significant clinical challenge. Conventional MRI, while sensitive, often lacks histopathological specificity. This study evaluates the synergistic diagnostic performance of advanced MRI techniques - Diffusion-Weighted Imaging (DWI) and Magnetic Resonance Spectroscopy (MRS) - in characterizing brain tumors, using histopathology as the gold standard.

Material and Method: This prospective observational study included 50 patients with suspected brain lesions. All patients underwent 3T MRI, including multi-sequence conventional imaging, axial DWI (b-values 0 and 1000 s/mm^2) for Apparent Diffusion Coefficient (ADC) mapping, and multi-voxel MRS (TE 35/144 ms). Key metabolite ratios (Cho/Cr, Cho/NAA, NAA/Cr) and ADC values were calculated from tumoral and peritumoral regions. These imaging findings were directly correlated with post-surgical histopathological diagnoses.

Result: Histopathology identified 35 malignant (70%) and 15 benign (30%) lesions. Malignant tumors demonstrated significantly lower mean ADC values and higher Choline (Cho) to Creatine (Cr) ratios. Receiver Operating Characteristic (ROC) analysis identified the Cho/Cr ratio as the most robust biomarker, yielding an Area Under the Curve (AUC) of 0.932 with a sensitivity of 94.3% and specificity of 86.7% at a cut-off of 1.72. The tumoral ADC value was also a strong differentiator (AUC 0.898), with a cut-off of 0.85 providing 94% sensitivity and 75% specificity. The combined use of DWI and MRS demonstrated a diagnostic accuracy of 86.0%, a sensitivity of 91.4%, and a specificity of 73.3%.

Conclusion: The integration of DWI and MRS provides a reliable and accurate non-invasive method for differentiating malignant and benign brain tumors. The Cho/Cr ratio, in particular, serves as a powerful and specific biomarker for malignancy. This synergistic approach enhances diagnostic confidence, aids in pre-surgical planning, and can help guide targeted biopsies.

Keywords*: Brain Tumors, Magnetic Resonance Imaging (MRI), Diffusion-Weighted Imaging (DWI), Apparent Diffusion Coefficient (ADC), Magnetic Resonance Spectroscopy (MRS), Choline/Creatine Ratio, Tumor Grading, Neuroradiology.*

INTRODUCTION

A brain tumor, an abnormal proliferation of cells within the cranium, presents a formidable diagnostic and therapeutic challenge. The incidence of central nervous system (CNS) tumors in India is reported to be between 5 and 10 per 100,000 population, with an increasing trend observed [7]. These tumors are highly heterogeneous, encompassing over 120 distinct types, ranging from benign (e.g., meningioma, pituitary adenoma) to highly malignant (e.g., glioblastoma, lymphoma). The primary clinical challenge lies in the accurate, non-invasive differentiation of these lesions. Distinguishing neoplastic from non-neoplastic lesions, and subsequently grading tumors, is critical as it dictates the entire management pathway, from neurosurgical intervention to chemotherapy and radiotherapy.

Conventional magnetic resonance imaging (MRI), including T1-weighted, T2-weighted, and fluid-attenuated inversion recovery (FLAIR) sequences, is the cornerstone of brain tumor detection. It provides exquisite anatomical detail regarding a lesion's size, location, and effect on adjacent structures. However, the specificity of conventional MRI is often limited. Features such as contrast enhancement, peritumoral edema, and mass effect can overlap significantly across different pathologies. For instance, a ring-enhancing lesion could represent a high-grade glioblastoma, a solitary metastasis, or a non-neoplastic abscess, creating a diagnostic dilemma [12].

This diagnostic ambiguity has driven the adoption of advanced, functional MRI techniques that provide physiological and biochemical information, moving beyond simple morphology. Diffusion-Weighted Imaging (DWI) and Magnetic Resonance Spectroscopy (MRS) have emerged as two of the most powerful tools in this domain [1]

Diffusion-Weighted Imaging (DWI) is a rapid and reproducible sequence that measures the random Brownian motion of water molecules [2]. The mobility of water in tissue is inversely correlated with tissue cellularity and cell membrane integrity [4]. In highly cellular tumors, such as lymphoma or high-grade gliomas, the dense packing of cells and a high nucleus-to-cytoplasm ratio restrict the diffusion of water. This restriction is quantified as a low Apparent Diffusion Coefficient (ADC) value. Conversely, tissues with lower cellularity or necrotic centers, like low-grade gliomas or certain cysts, exhibit higher water mobility and thus higher ADC values [3]

Magnetic Resonance Spectroscopy (MRS) provides a "molecular window" into tissue biochemistry, non-invasively quantifying the relative concentrations of key brain metabolites [8]. In neuro-oncology, a characteristic metabolic signature is often observed :

- **N-acetyl aspartate (NAA):** A marker of neuronal viability, its peak (at 2.0 ppm) is typically *decreased* in tumors as neoplastic cells displace or destroy normal neurons [5].
- **Choline (Cho):** A marker of cell membrane turnover and proliferation, its peak (at 3.2 ppm) is *elevated* in malignant tumors due to rapid cell division and synthesis of new cell membranes [6]
- **Creatine (Cr):** A marker of cellular energy metabolism (peak at 3.0 ppm), it tends to be relatively stable and is often used as an internal reference.
- **Lipids and Lactate:** Peaks in the 0.9-1.3 ppm range are markers of anaerobic glycolysis and cell membrane breakdown (necrosis), respectively. Their presence is often indicative of high-grade, aggressive tumors [9].

The central hypothesis of this study is that DWI (providing data on cellularity) and MRS (providing data on metabolic activity) are complementary. Their synergistic use should provide a more accurate and robust non-invasive "signature" for brain tumors than either technique alone. While numerous studies have evaluated these modalities individually, this study aims to prospectively quantify their combined diagnostic performance against the gold standard of histopathology in a diverse cohort of 50 patients.

AIMS AND OBJECTIVE

This study was planned with the aim of establishing the usefulness of Diffusion-Weighted MRI (DW-MRI) and MR Spectroscopy in the differentiation of brain tumors into benign and malignant categories, and to further associate the imaging findings with the final histopathological results.

The objectives of the study were :

1. To determine the usefulness of diffusion-weighted MRI in the characterization of brain tumors into benign and malignant lesions.
2. To determine the usefulness of Magnetic Resonance Spectroscopy in the evaluation of brain tumors.
3. To correlate the findings of DWI and MRS with histopathological results.

MATERIAL AND METHOD

Study Design and Ethical Approval

This prospective, observational study was conducted in the Department of Radio-diagnosis, Mahatma Gandhi Medical College & Hospital, Jaipur. The study protocol was approved by the Institutional Ethics Committee (IEC). All participants provided written informed consent prior to inclusion in the study, in accordance with the Declaration of Helsinki.

Patient Cohort

A minimum sample size of 50 patients was targeted. Patients presenting with clinical symptoms suggestive of a brain tumor, who were referred for a contrast-enhanced MRI of the brain, were enrolled.

Inclusion Criteria: All patients presenting with symptoms of brain tumors.

Exclusion Criteria: Patients with claustrophobia, those who were hemodynamically unstable, individuals with tremors or movement disorders preventing a motion-free scan, and patients who refused to give consent.

Imaging Protocol
All examinations were performed on a 3 Tesla (3T) MRI system. The comprehensive protocol included conventional T1-weighted, T2-weighted, FLAIR, and post-contrast T1-weighted sequences, supplemented by the following advanced sequences :

Diffusion-Weighted Imaging (DWI):
DWI was performed using an axial echo-planar spin-echo (SE) sequence. Images were acquired with b-values of 0 and 1000 s/mm^2 using a 5 mm section thickness. Apparent Diffusion Coefficient (ADC) maps were automatically generated from the DWI data. Regions of Interest (ROIs) were placed on the solid, non-necrotic/non-cystic portions of the tumor, and mean ADC values (expressed in 10^{-3}mm^2/s) were calculated.

Magnetic Resonance Spectroscopy (MRS):
Multi-voxel MR spectroscopy was performed using a spin-echo (SE) mode sequence with both a short echo time (TE) of 35 ms and a long TE of 144 ms. Water suppression was achieved using a Chemical Shift Selection (CHESS) technique. Voxels were placed over the solid part of the lesion, in the perilesional area, and in a corresponding normal region of the contralateral hemisphere for comparison. Metabolite peaks were identified, including N-acetyl aspartate (NAA) at 2.0 ppm, Creatine (Cr) at 3.0 ppm, Choline (Cho) at 3.2 ppm, Lactate at 1.33 ppm, and Lipids (0.7-1.3 ppm). The key metabolite ratios (Cho/NAA, Cho/Cr, NAA/Cr) were calculated from the intra-lesional spectra.

Histopathological Correlation
The final diagnosis for all 50 patients was obtained from post-operative or stereotactic biopsy specimens. The imaging findings were correlated with the histopathological diagnosis, which served as the gold standard for classifying lesions as benign or malignant.

Statistical Analysis
All data were entered into an Excel spreadsheet and analyzed using IBM SPSS Statistics version 29. Descriptive statistics (mean standard deviation for continuous variables, frequencies and percentages for categorical variables) were calculated. An independent-samples t-test was used to compare means between two groups, while a one-way ANOVA was used for comparisons across more than two groups. A Chi-square test was used for associations between categorical variables. A P-value less than 0.05 was considered statistically significant.

Receiver Operating Characteristic (ROC) curve analysis was performed to determine the optimal cut-off values for ADC and metabolite ratios in differentiating benign from malignant lesions. The Area Under the Curve (AUC), sensitivity, specificity, positive predictive value (PPV), and negative predictive value (NPV) were calculated to assess the diagnostic performance of each parameter and the combined protocol.

RESULTS
Patient Demographics and Tumor Classification
The study cohort comprised 50 patients with a mean age of 51 ± 12.5 years (range, 26-68 years). The majority of patients (68%) were in the >50 years age group.

Table 1: Age Distribution

Age Group (years)	N	Percentage
20-30	4	8.0%
30-40	8	16.0%
40-50	4	8.0%
>50	34	68.0%
Total	**50**	**100.0%**

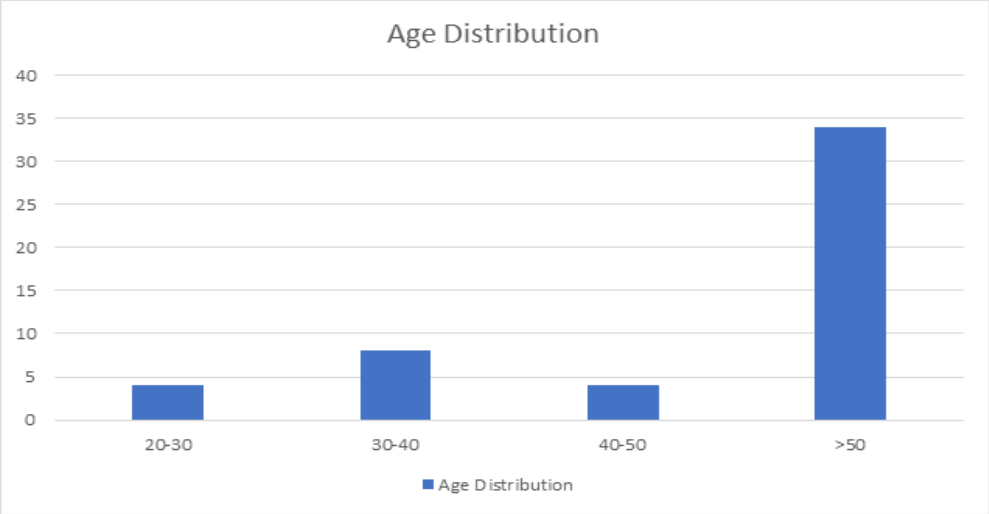

Figure 1: Age Distribution (Histogram - showing the frequency of patients in age groups: 20-30 (8%), 30-40 (16%), 40-50 (8%), and >50 (68%).)

There was a male predominance, with 30 males (60%) and 20 females (40%). The mean age was not significantly different between males (50.3 ± 14.7 years) and females (51.7 ± 9.9 years) (P=0.718).

Table 2: Gender Distribution

Gender	**N**	**Percentage**
Male	30	60.0%
Female	20	40.0%
Total	**50**	**100.0%**

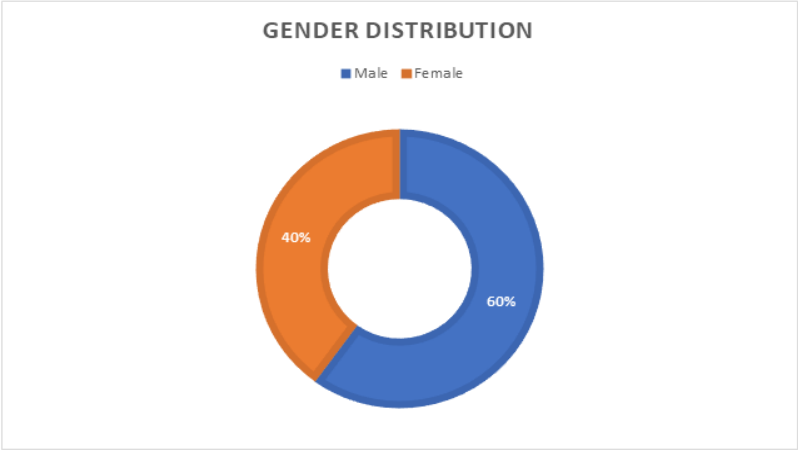

Figure 2: Gender Distribution (Pie Chart - illustrating the gender split: 60% Male, 40% Female.)

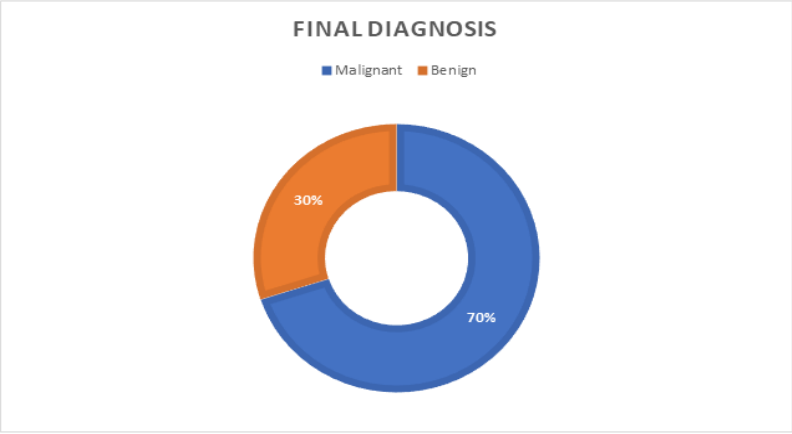

Figure 3: Histopathology confirmed Final Diagnosis - (Pie Chart - illustrating 35 (70%) malignant and 15 (30%) benign lesions.)

The initial radiological diagnoses and final histopathological diagnoses were cataloged.

Table 3: Brain Tumour Type (Initial MRI Diagnosis)

Tumour type	N	Percentage
Glioma	4	8.0%
Glioblastoma MF	5	10.0%
Meningioma	8	16.0%
Lymphoma	8	16.0%
Metastasis	9	18.0%
Astrocytoma	4	8.0%
Neuroblastoma	4	8.0%
Medulloblastoma	4	8.0%
Oligodendroglioma	4	8.0%
Total	**50**	**100.0%**

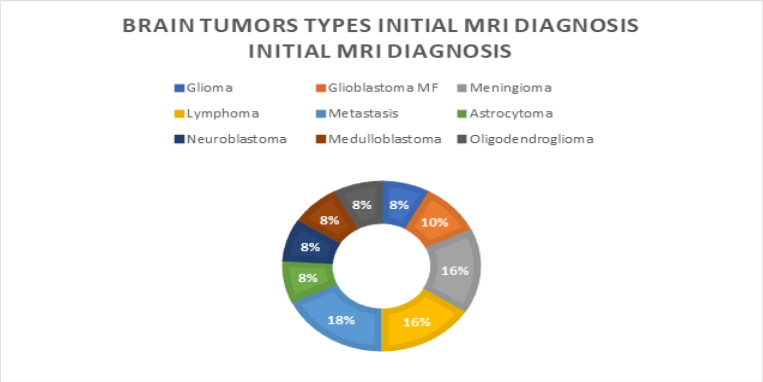

Figure 4: Type of Tumors (MRI) (A pie chart showing the distribution of initial MRI diagnoses, with Metastasis (18%), Meningioma (16%), and Lymphoma (16%) as the most common.)

Table 4: Tumour Type (MRI Diagnosis) and Age

Tumour Type	20-30	30-40	40-50	>50
Glioma	0	0	0	4
Glioblastoma MF	0	0	0	5
Meningioma	0	0	0	8
Lymphoma	0	0	0	8
Metastasis	0	0	0	9
Astrocytoma	0	4	0	0
Neuroblastoma	4	0	0	0
Medulloblastoma	0	4	0	0
Oligodendroglioma	0	4	0	0
Total	**4**	**8**	**4**	**34**

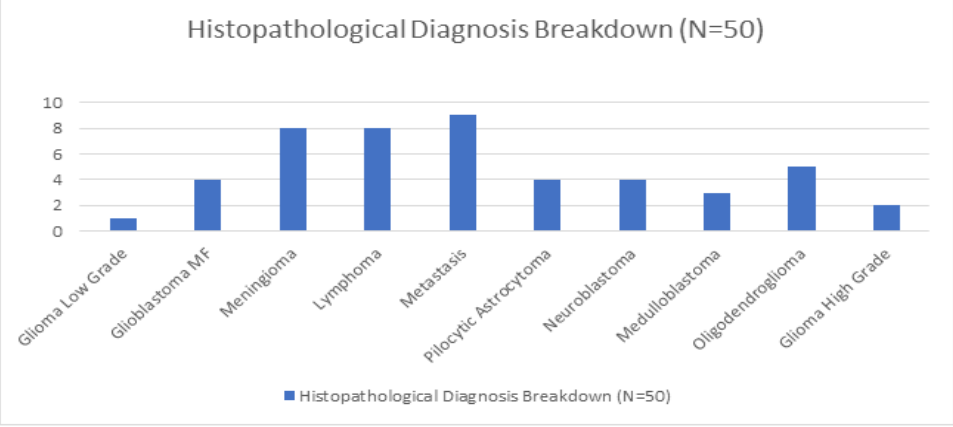

Figure 5: A bar chart showing Metastasis, Meningioma, and Lymphoma were the most common diagnoses, each accounting for 16-18% of the cohort. This diverse mix provides a robust test for the imaging techniques.

The final cohort, based on histopathology, consisted of 35 malignant (70%) and 15 benign (30%) lesions.

Table 5: Distribution of Histopathological Diagnoses

Histopathological Diagnosis	N	Percentage
Glioma Low Grade	1	2.0%
Glioblastoma MF	4	8.0%
Meningioma	8	16.0%
Lymphoma	8	16.0%
Metastasis	9	18.0%
Pilocytic Astrocytoma	4	8.0%
Neuroblastoma	4	8.0%
Medulloblastoma	3	6.0%
Oligodendroglioma	5	10.0%
Glioma High Grade	2	4.0%
Total	**50**	**100.0%**

Table 6: Histopathological Diagnosis and Age Group

Tumour Type	20-30	30-40	40-50	>50
Glioma LG	0	0	0	1*
Glioblastoma MF	0	0	0	4
Meningioma	0	0	0	8
Lymphoma	0	0	0	8
Metastasis	0	0	0	9
Pilocytic Astrocytoma	0	0	4	0
Neuroblastoma	4	0	0	0
Medulloblastoma	0	3	0	0
Oligodendroglioma	0	5	0	0
Glioma HG	0	0	0	2
Total	**4**	**8**	**4**	**34**

Table 6a: Imaging Characteristics by Histopathological Type

Tumor Type	T1WI (Iso/Hypo)	T2WI (Hyper)	FLAIR (Hyper)	Diffusion restriction (Present)	Blooming on GRE (Present)	Contrast enhancement (Present)
Glioma Low Grade	2/3	1/3	2/3	1/3	1/3	2/3
Glioma High Grade	1/2	2/3	2/3	2/3	2/3	3/3
Meningioma	4/8	2/8	3/8	6/8	6/8	8/8
Lymphoma	5/9	5/9	5/9	9/9	9/9	9/9
Metastasis	3/8	2/8	3/8	3/8	3/8	8/8
Pilocytic Astrocytoma	3/4	3/4	3/4	0/4	2/4	4/4
Neuroblastoma	2/4	2/4	2/4	2/4	1/4	3/4
Medulloblastoma	3/3	3/3	2/3	2/3	1/3	2/3
Oligodendroglioma	4/5	4/5	4/5	4/5	1/5	4/5
Glioblastoma MF	2/4	3/4	3/4	3/4	3/4	4/4
Values expressed as N / Total N for that tumor type						

DWI Analysis and ADC Quantification

Tumoral ADC:

A statistically significant difference (ANOVA, $P<0.001$) was observed in the mean ADC values among different tumor types. Malignant tumors, particularly those with high cellularity, demonstrated the lowest ADC values. Lymphoma had the lowest mean ADC ($0.5 \pm 0.11 \times 10^{-3} mm^2/s$), followed by Metastasis ($0.64 \pm 0.02 \times 10^{-3} mm^2/s$) and Glioblastoma MF ($0.78 \pm 0.11 \times 10^{-3} mm^2/s$). Benign lesions demonstrated significantly higher ADC values, with Pilocytic Astrocytoma showing the highest mean ADC ($1.5 \pm 0.1 \times 10^{-3} mm^2/s$).

Table 7: Mean Tumoral ADC Values by Tumor Type

Tumor Type (Histopathology)	Mean ADC (×10−3mm2/s) ± SD
Glioma (LG/HG)	1.24 ± 0.02
Glioblastoma MF	0.78 ± 0.11
Meningioma	0.85 ± 0.13

Lymphoma	0.50 ± 0.11
Metastasis	0.64 ± 0.02
Pilocytic Astrocytoma	1.50 ± 0.1
Neuroblastoma	1.00 ± 0.1
Medulloblastoma	1.03 ± 0.11
Oligodendroglioma	1.20 ± 0.1

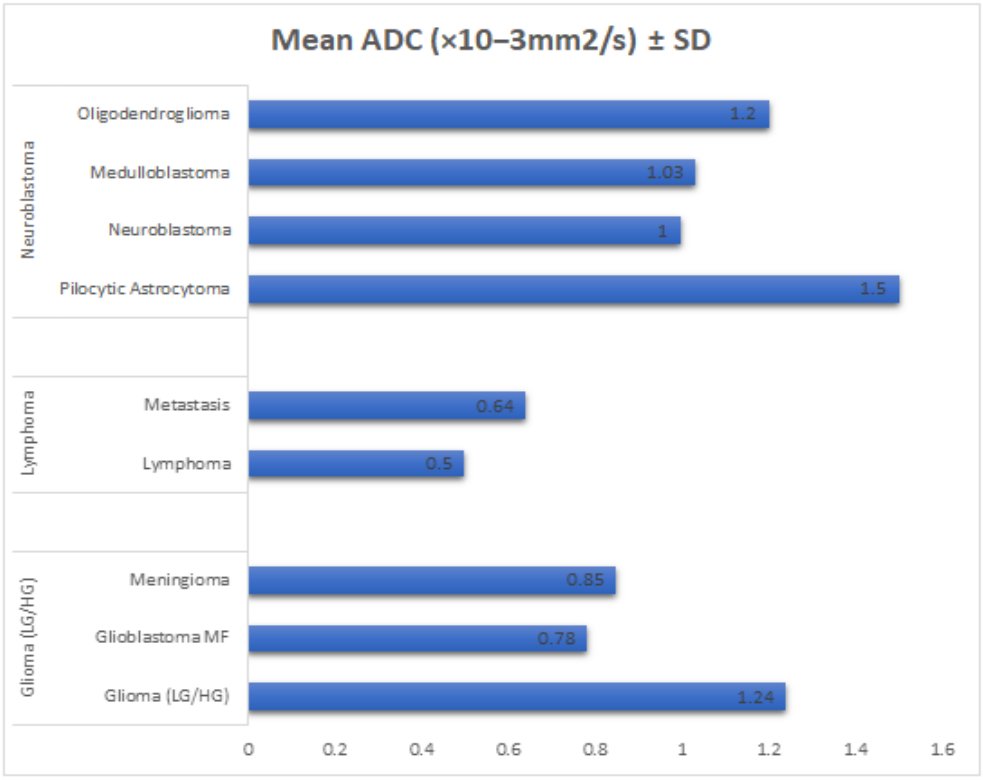

Figure 6: Mean Tumoral ADC Values (A bar chart showing the mean ADC values for each tumor type, highlighting the low values for Lymphoma (0.50) and Metastasis (0.64) and the high value for Pilocytic Astrocytoma (1.50).)

Peritumoral ADC:

Analysis of the peritumoral region also yielded significant differences ($P<0.001$). Infiltrative tumors like Glioma showed a high mean peritumoral ADC ($1.8 \pm 0.1 \times 10^{-3}$ mm^2/s), reflecting neoplastic infiltration. In contrast, well-circumscribed tumors like Metastasis, which produce vasogenic edema, showed a significantly lower mean peritumoral ADC ($1.36 \pm 0.01 \times 10^{-3}$ mm^2/s).

Table 8: Mean Peritumoral ADC Values by Tumor Type

Tumor Type (Histopathology)	**Mean Peritumoral ADC (×10−3mm2/s) ± SD**
Glioma (LG/HG)	1.80 ± 0.1
Glioblastoma MF	1.41 ± 0.2
Meningioma	1.43 ± 0.03
Lymphoma	1.40 ± 0.06
Metastasis	1.36 ± 0.01
Pilocytic Astrocytoma	1.70 ± 0.1
Neuroblastoma	1.60 ± 0.2
Medulloblastoma	1.49 ± 0.15
Oligodendroglioma	1.60 ± 0.12

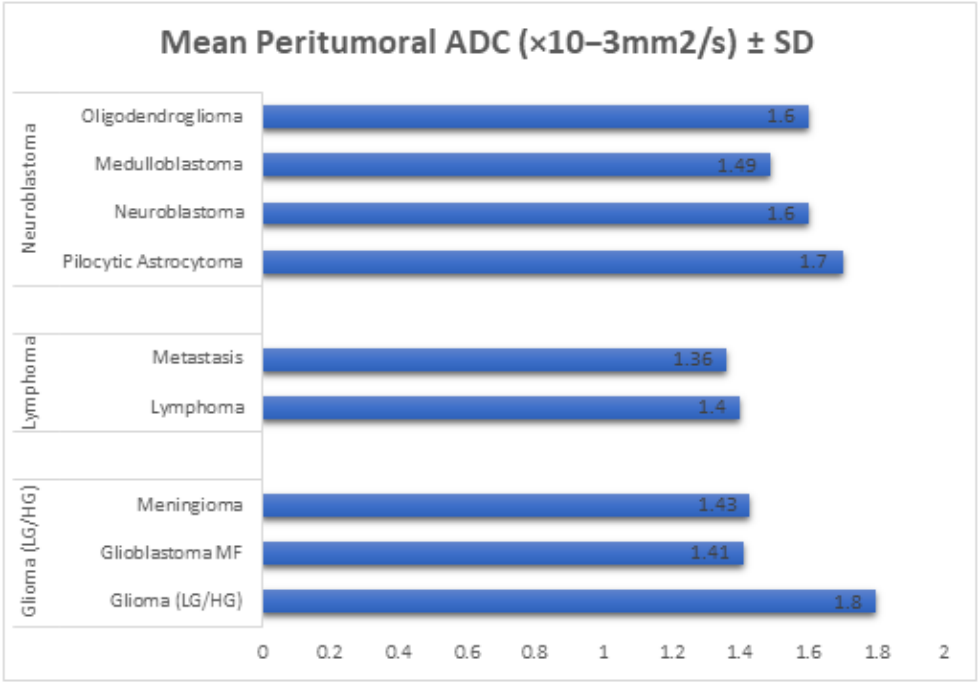

Figure 7: Mean Peritumoral ADC Values (A bar chart showing the mean peritumoral ADC values, with Glioma (1.80) and Pilocytic Astrocytoma (1.70) having the highest values, and Metastasis (1.36) having the lowest.)

MRS Metabolite Analysis

Metabolite Ratios:

All three calculated metabolite ratios showed statistically significant differences among tumor types (ANOVA, P<0.001).

- **NAA/Cr Ratio:** This ratio, a marker of neuronal integrity, was lowest in highly aggressive tumors like Metastasis (0.1 ± 0.01) and Glioblastoma MF (0.88 ± 0.48), and highest in slower-growing or benign lesions like Medulloblastoma (2.9 ± 0.8) and Pilocytic Astrocytoma (2.4 ± 1).
- **Cho/Cr Ratio:** This ratio, a marker of cell proliferation, was markedly elevated in malignant tumors. Metastasis showed the highest mean ratio (4.1 ± 1.4), followed by Lymphoma (3.3 ± 0.1) and Glioblastoma MF (2.5 ± 0.1). Benign and low-grade tumors showed ratios closer to 1.0 (e.g., Pilocytic Astrocytoma, 1.02 ± 1.3).
- **Cho/NAA Ratio:** This ratio, combining the markers of proliferation and neuronal loss, was also elevated in malignancy. Pilocytic Astrocytoma (2.8 ± 0.4) showed a high ratio, as did Lymphoma (2.5 ± 0.6) and Metastasis (2.3 ± 0.6). Less aggressive tumors like Neuroblastoma (1.4 ± 0.1) had lower ratios.

Table 9: Mean NAA/Cr Ratio by Tumor Type

Tumor Type (Histopathology)	Mean NAA/Cr Ratio ± SD
Glioma (LG/HG)	1.66 ± 0.06
Glioblastoma MF	0.88 ± 0.48
Meningioma	1.70 ± 0.6
Lymphoma	1.50 ± 0.3
Metastasis	0.10 ± 0.01
Pilocytic Astrocytoma	2.40 ± 1
Neuroblastoma	2.30 ± 0.02
Medulloblastoma	2.90 ± 0.8
Oligodendroglioma	2.50 ± 1

Table 10: Mean Cho/Cr Ratio by Tumor Type

Tumor Type (Histopathology)	Mean Cho/Cr Ratio ± SD
Glioma (LG/HG)	1.39 ± 0.7
Glioblastoma MF	2.50 ± 0.1
Meningioma	2.43 ± 1.5
Lymphoma	3.30 ± 0.1
Metastasis	4.10 ± 1.4
Pilocytic Astrocytoma	1.02 ± 1.3
Neuroblastoma	0.37 ± 0.01
Medulloblastoma	1.00 ± 0.8
Oligodendroglioma	1.70 ± 0.1

Table 11: Mean Cho/NAA Ratio by Tumor Type

Tumor Type (Histopathology)	Mean Cho/NAA Ratio ± SD
Glioma (LG/HG)	2.10 ± 0.6
Glioblastoma MF	2.30 ± 0.8
Meningioma	2.20 ± 0.5
Lymphoma	2.50 ± 0.6
Metastasis	2.30 ± 0.6
Pilocytic Astrocytoma	2.80 ± 0.4
Neuroblastoma	1.40 ± 0.1
Medulloblastoma	1.40 ± 0.3
Oligodendroglioma	1.70 ± 0.3

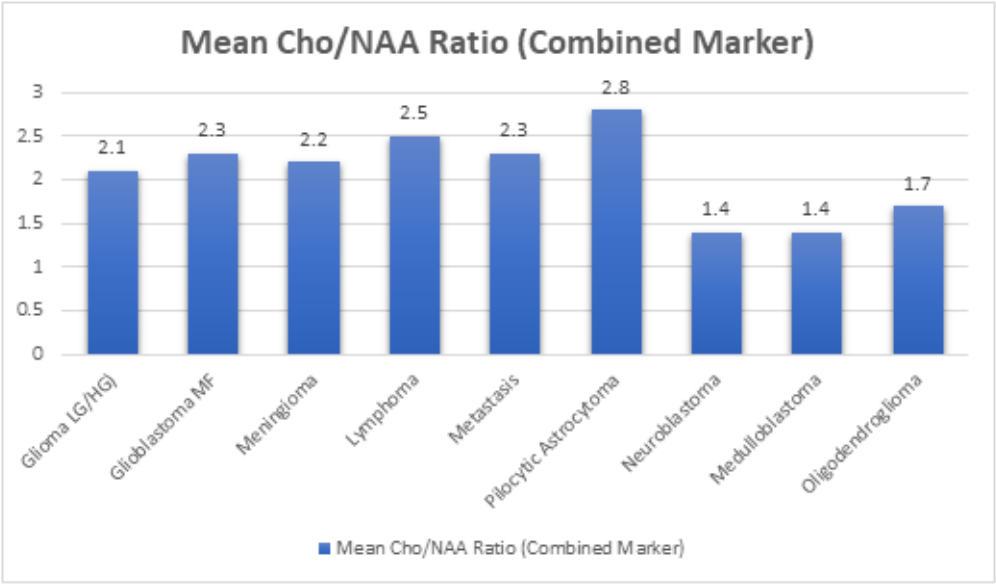

Figure 8: Mean Cho/NAA Ratio (A bar chart showing the mean Cho/NAA ratio, with most malignant tumors (GBM, Lymphoma, Metastasis) clustering between 2.3-2.5 and Pilocytic Astrocytoma (2.80) being the highest.)

Lipid and Lactate Peak Analysis:

The presence of Lactate was non-specific, appearing in 35/50 cases (70%) and was seen in both high-grade (80% of GBMs, 100% of Lymphomas) and low-grade lesions (100% of Pilocytic Astrocytomas), indicating its relation to anaerobic glycolysis in general (P=0.037).

However, the presence of a Lipid peak was a strong indicator of high-grade malignancy and necrosis (P<0.001). Lipids were present in 22/50 cases (44%), including 100% of Lymphomas (8/8), 80% of Glioblastomas (4/5), and 67% of Metastases (6/9). Conversely, lipid peaks were absent in 100% of Pilocytic Astrocytomas, Neuroblastomas, and Oligodendrogliomas.

Table 12: Lactate Presence by Tumor Type

Tumor Type	Present (N)	Absent (N)
Glioma (LG/HG)	2	2
Glioblastoma MF	4	1
Meningioma	6	2
Lymphoma	8	0
Metastasis	6	3
Pilocytic Astrocytoma	4	0
Neuroblastoma	0	4*
Medulloblastoma	2	1*
Oligodendroglioma	3	2
Total	**35 (70%)**	**15 (30%)**

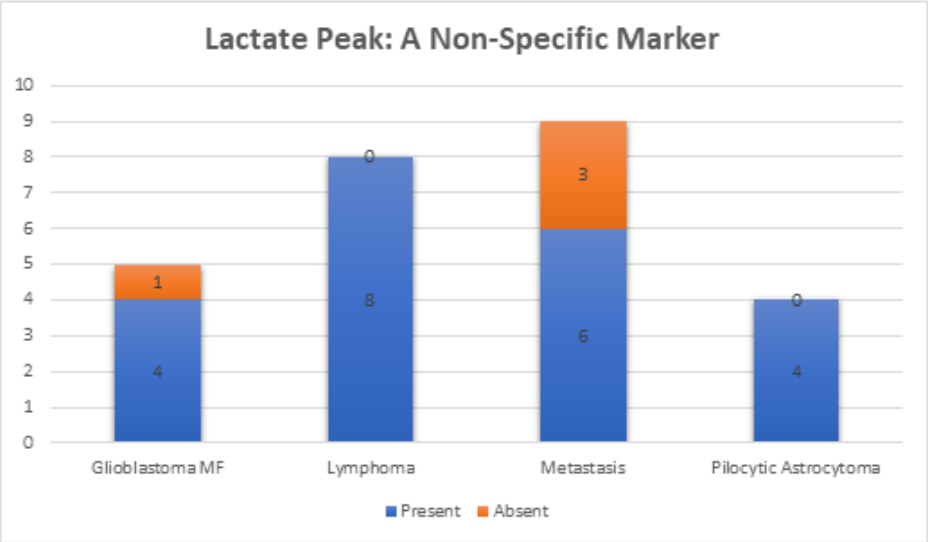

Figure 9: Lactate Presence (A bar chart showing the count of "Positive" vs. "Negative" lactate peaks for each tumor type.) Lactate, a marker for anaerobic glycolysis, was less specific. It was found in 70% of all cases, appearing in both high-grade lesions (100% of Lymphomas) and benign ones (100% of Pilocytic Astrocytomas).

Table 13: Lipid Presence by Tumor Type

Tumor Type	Present (N)	Absent (N)
Glioma (LG/HG)	2	2
Glioblastoma MF	4	1
Meningioma	0	8
Lymphoma	8	0
Metastasis	6	3
Pilocytic Astrocytoma	0	4
Neuroblastoma	0	4
Medulloblastoma	2	1*
Oligodendroglioma	0	5*
Total	**22 (44%)**	**28 (56%)**

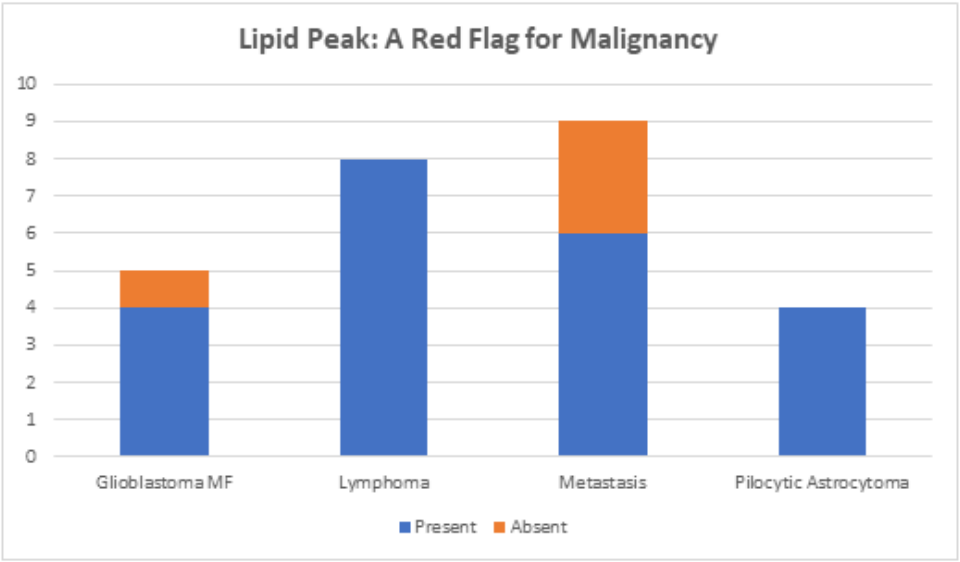

Figure 10: Lipid Presence (A bar chart showing the count of "Positive" vs. "Negative" lipid peaks, highlighting the 100% presence in Lymphoma and 0% presence in Meningioma, Pilocytic Astrocytoma, Neuroblastoma, and Oligodendroglioma.)

Diagnostic Performance (ROC Analysis)

ROC curve analysis was used to determine the diagnostic utility of the most significant ADC and metabolite parameters for differentiating benign from malignant lesions. The analysis clearly identifies the **Cho/Cr ratio** as the single most powerful and balanced biomarker in this study, possessing the highest AUC (0.932).

Table 14: ADC (Area Under the Curve)

Area (AUC)	Std. Error	P-value	95% Confidence Interval
.898	.046	<.001	.807 -.988

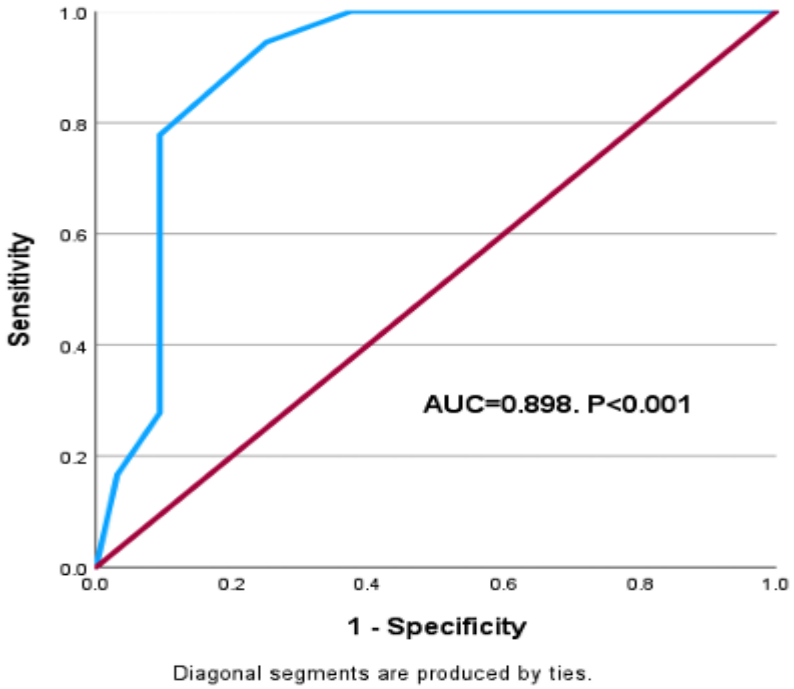

Figure 11: ADC ROC Curve
(A ROC curve for Tumoral ADC, showing an AUC of 0.898 (P<0.001).)

Table 15: NAA/Cr Ratio (Area Under the Curve)

Area (AUC)	Std. Error	P-value	95% Confidence Interval
.874	.052	<.001	.773 -.975

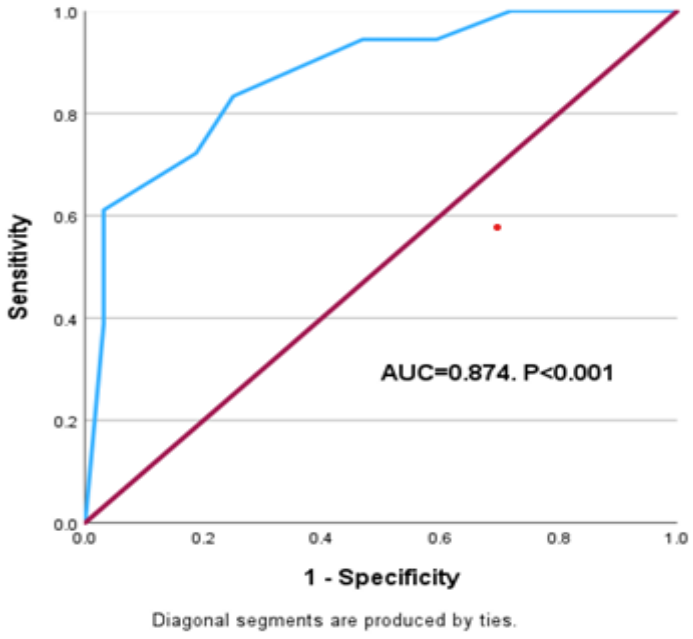

Figure 12: NAA/Cr ROC Curve
(A ROC curve for NAA/Cr ratio, showing an AUC of 0.874 (P<0.001).)

Table 16: Cho/Cr Ratio (Area Under the Curve)

Area (AUC)	Std. Error	P-value	95% Confidence Interval
.932	.038	<.001	.857 - 1.000

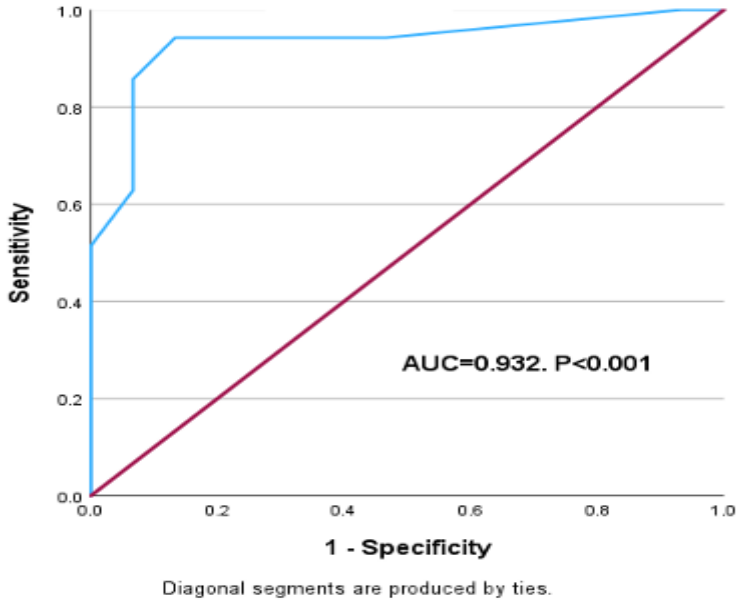

Figure 13: Cho/Cr ROC Curve
(A ROC curve for Cho/Cr ratio, showing an AUC of 0.932 (P<0.001).)

Table 17: Cho/NAA Ratio (Area Under the Curve)

Area (AUC)	Std. Error	P-value	95% Confidence Interval
.710	.087	.020	.539 -.880

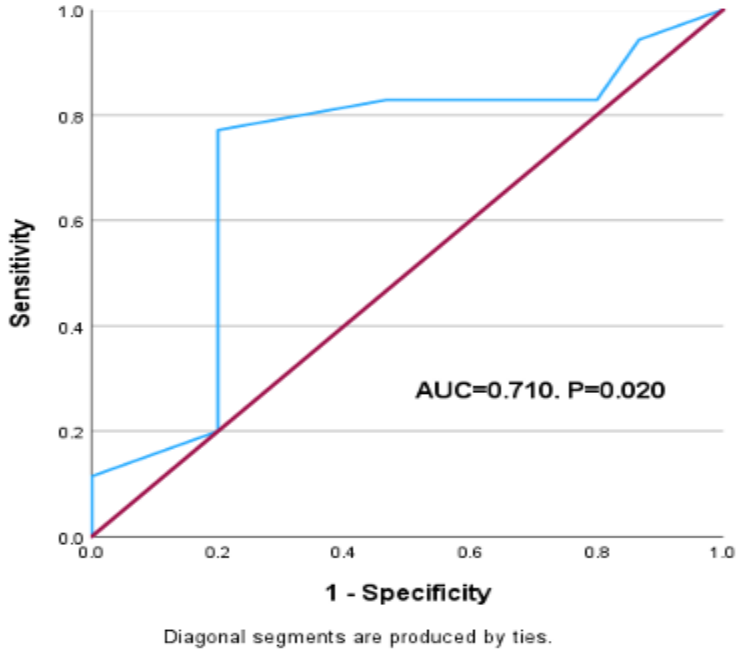

Figure 14: Cho/NAA ROC Curve
(A ROC curve for Cho/NAA ratio, showing an AUC of 0.710 (P=0.020).)
The consolidated performance metrics at the optimal cut-off values are presented in Table 18.

Table 18: Diagnostic Performance of Key Imaging Parameters (from ROC Analysis)

Parameter	Cut-off Value	Sensitivity	Specificity	AUC
Cho/Cr Ratio	**1.72**	**94.3%**	**86.7%**	**0.932**
ADC (Tumor)	0.85	94.0%	75.0%	0.898
NAA/Cr Ratio	1.60	83.3%	73.0%	0.874
Cho/NAA Ratio	1.86	77.1%	80.0%	0.710

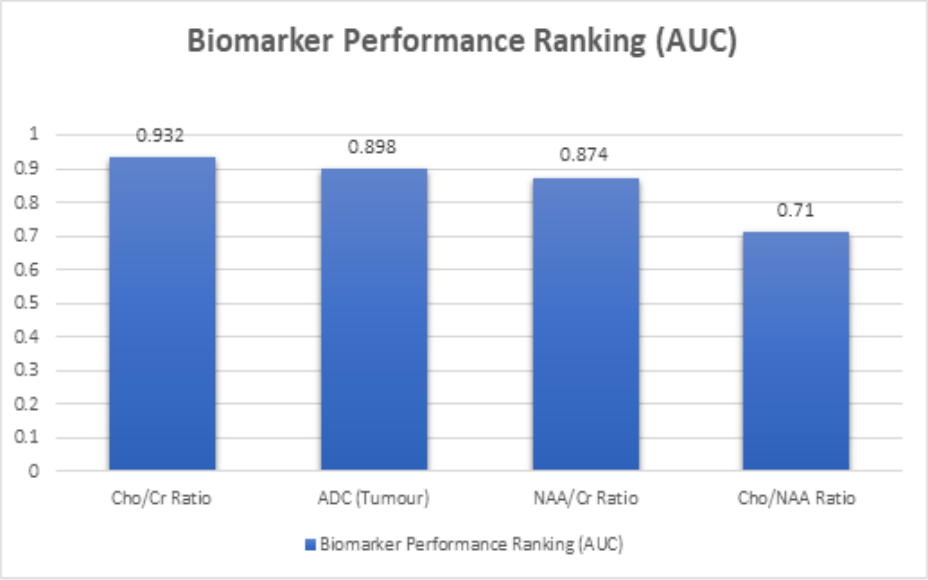

Figure 15: A bar chart showing Biomarker Performance Ranking (AUC) - ROC analysis - optimal cut-off for each metric and its ability to differentiate benign from malignant lesions. An Area Under the Curve (AUC) of 1.0 is a perfect test.

The Cho/Cr ratio was the clear winner, with the highest AUC (0.932), indicating the best balance of sensitivity and specificity for diagnosing malignancy.

Combined Protocol Accuracy

When DWI and MRS findings were combined (Table 19), the protocol correctly identified 32 of 35 malignant lesions (true positives) and 11 of 15 benign lesions (true negatives). There were 4 false positives and 3 false negatives.

Table 19: Diagnostic Performance of Combined DWI and MRS

Parameter	**Value**
Sensitivity	91.4%
Specificity	73.3%
Diagnostic Accuracy	**86.0%**
Positive predictive value (PPV)	88.9%
Negative predictive value (NPV)	78.6%

Illustrative Case Series

The quantitative findings are visually substantiated by the following representative cases from the study.

Case Illustration 1 : Metastasis

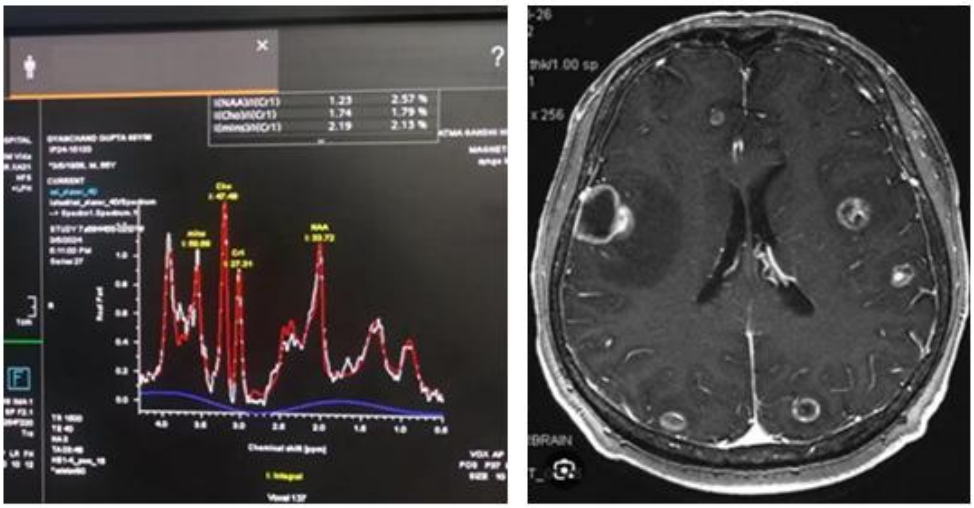

MRS spectrum demonstrates elevated choline and creatine peaks, with a resultant increased Cho/Cr ratio, characteristic of a metastatic lesion.

Case Illustration 2 : Glioblastoma Multiforme

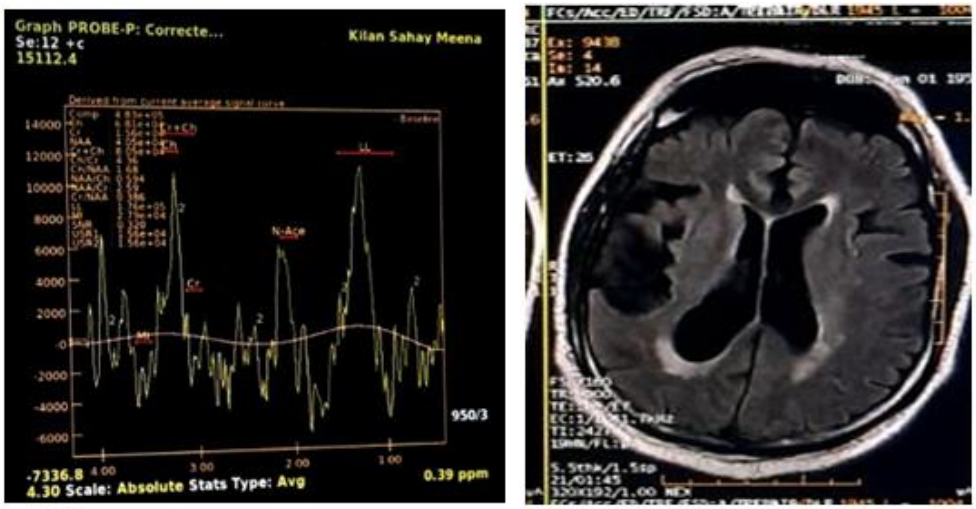

MRS shows elevated choline, mildly reduced creatine and NAA, and prominent elevated peaks for lipid and lactate, a classic signature for high-grade, necrotic glioblastoma.

Case Illustration 3 : Meningioma

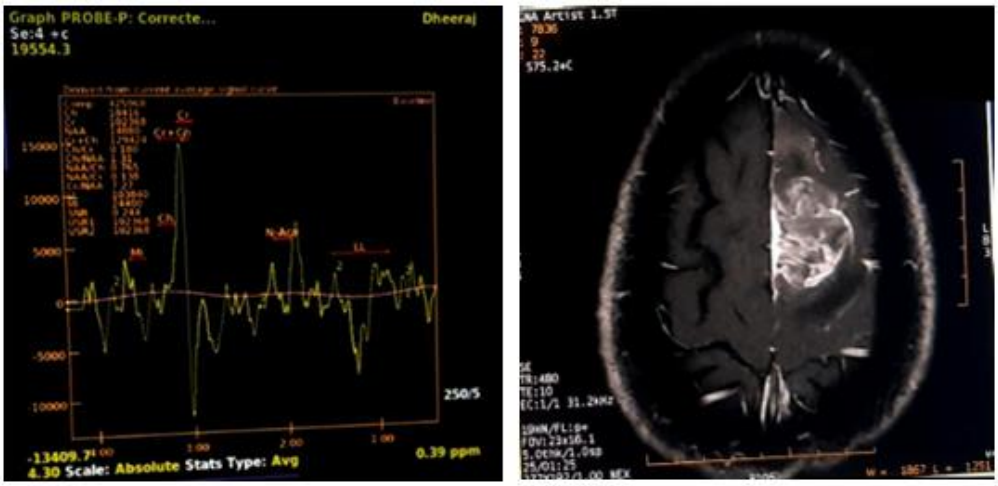

A right parietal meningioma showing elevated choline and creatine peaks with mildly reduced NAA on MRS.

Case Illustration 4 : Oligodendroglioma

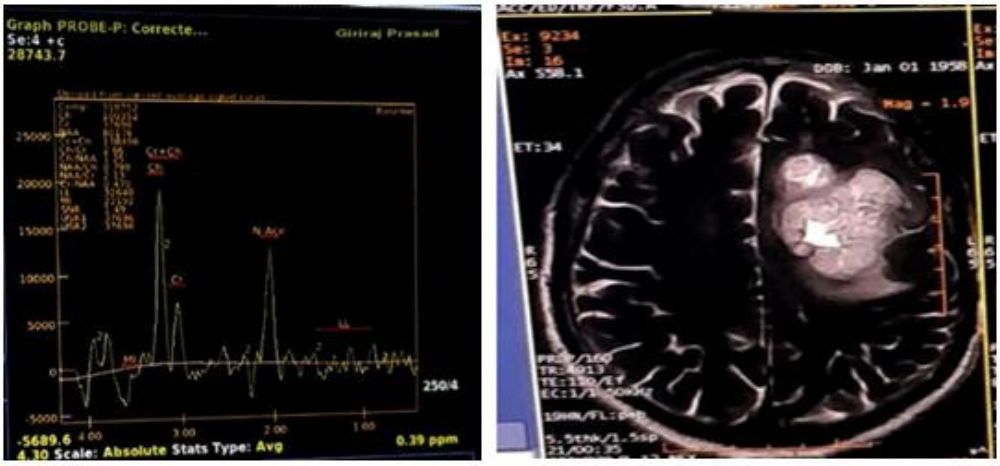

A right parietal oligodendroglioma. The MRS spectrum clearly shows an elevated choline peak with a corresponding reduction in NAA.

Case Illustration 5 : Neuroblastoma

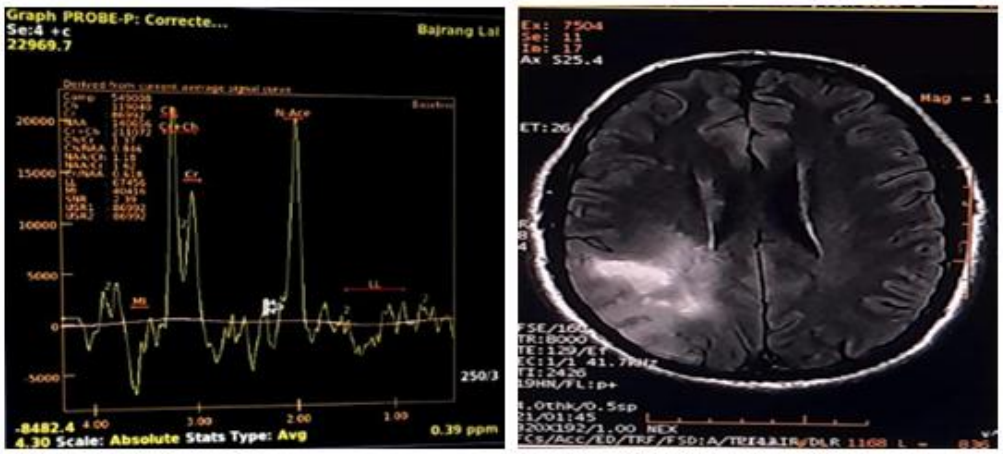

A left temporo-occipital neuroblastoma. MRS reveals a high choline peak, leading to increased Cho/Cr and Cho/NAA ratios.

Case Illustration 6 : Lymphoma

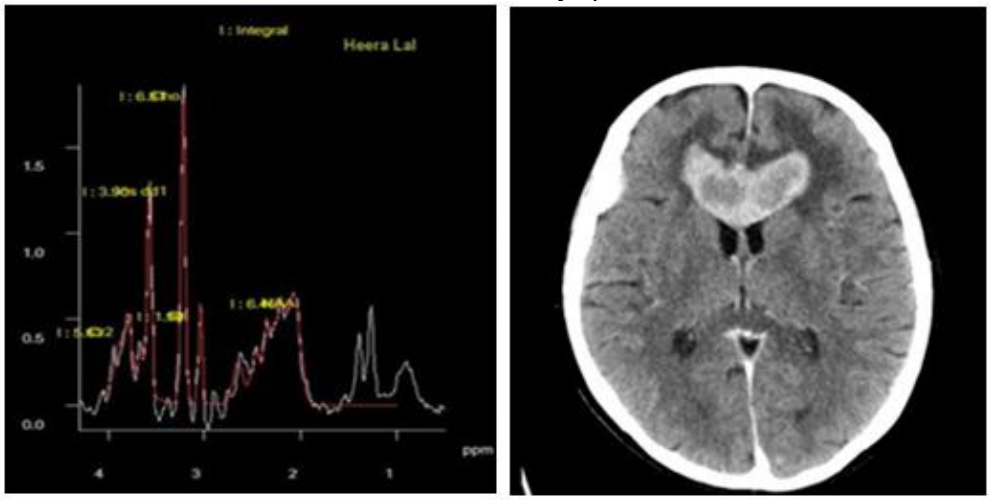

Spectrum from a lymphoma, demonstrating a markedly elevated choline peak and a significantly reduced NAA peak.

Case Illustration 7 : Glioblastoma Multiforme

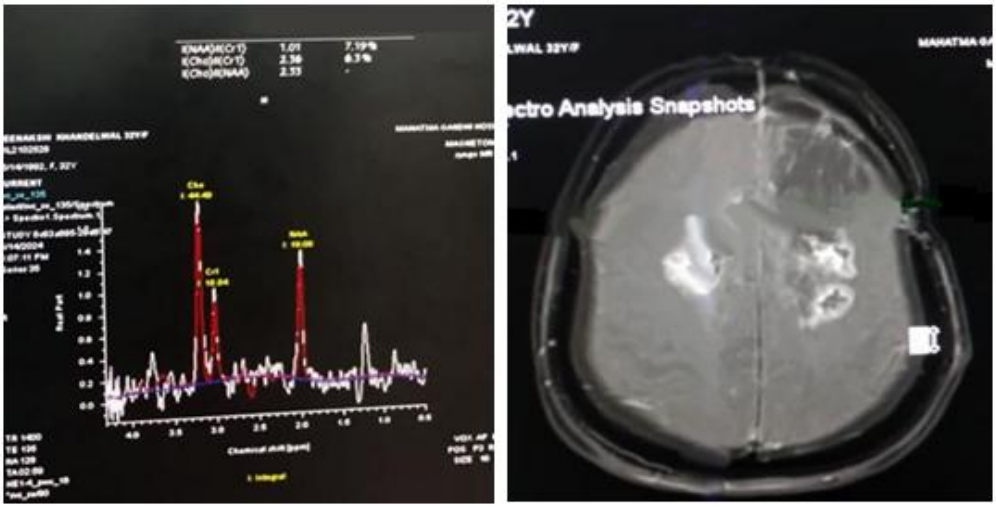

MRS shows increased choline, lipid, and lactate peaks with a reduced Cho/NAA ratio, indicative of a high-grade Glioblastoma Multiforme.

Case Illustration 8 : Metastasis

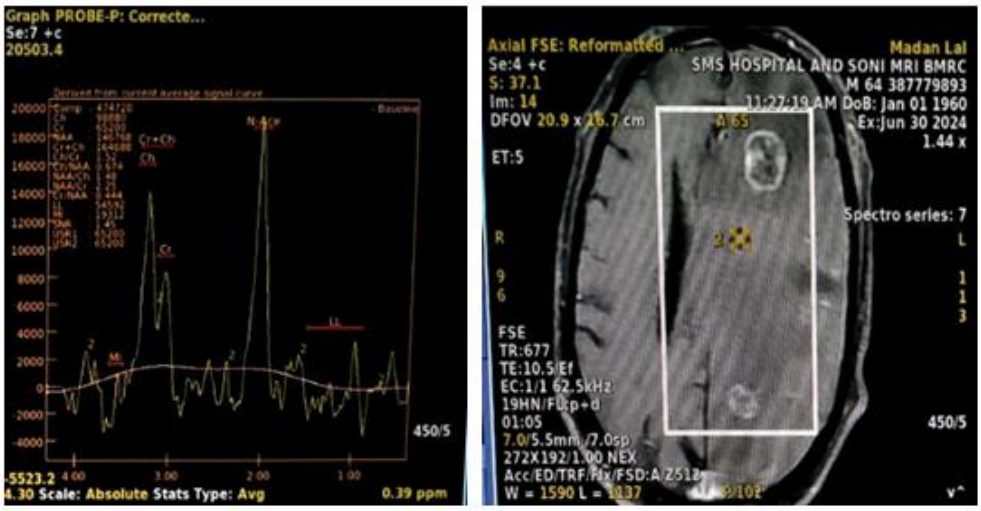

A case of metastasis showing significantly elevated choline peaks, mildly reduced creatine and NAA, and elevated lipid and lactate peaks, suggesting an aggressive lesion.

Case Illustration 9 : Metastasis

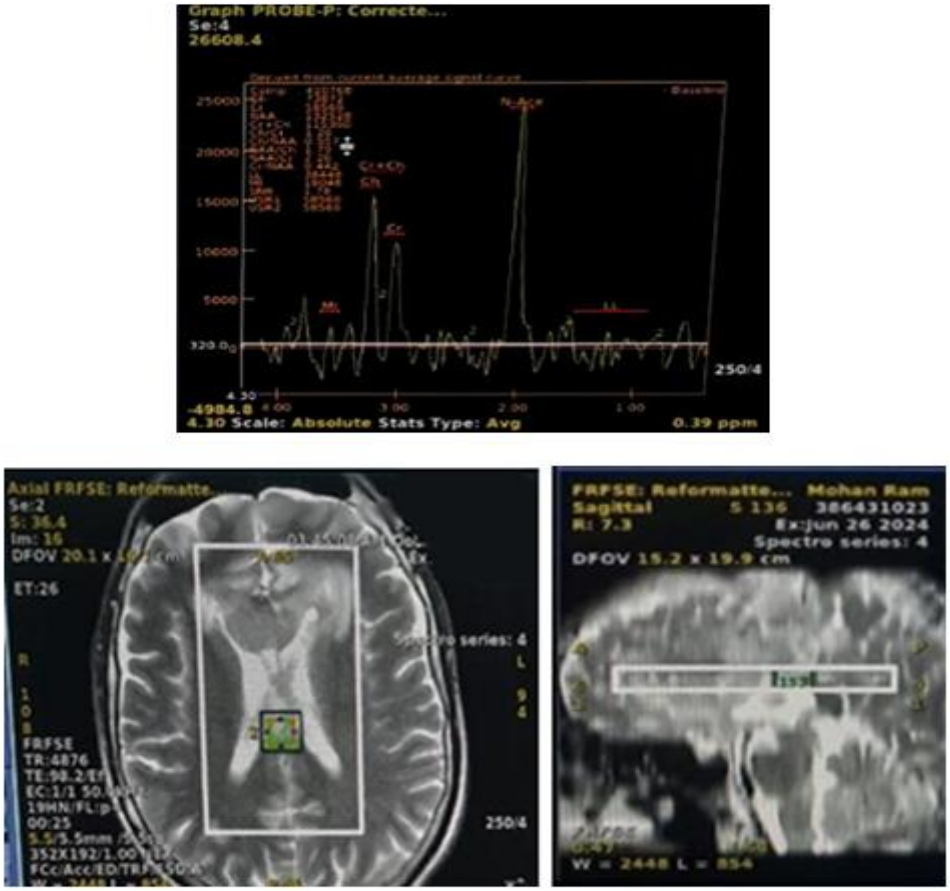

This metastatic lesion demonstrates elevated choline peaks with reduced NAA and creatine. Both the Cho/Cr and Cho/NAA ratios are increased.

Case Illustration 10 : Glioma

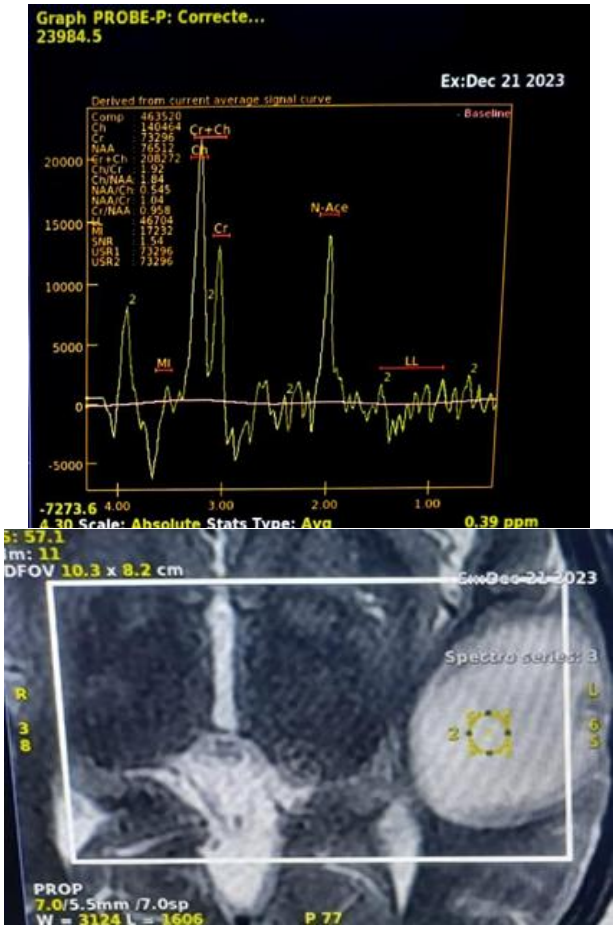

A glioma exhibiting increased choline and lactate peaks with low creatine and NAA levels on MRS.

DISCUSSION

This prospective study confirms the significant, synergistic value of integrating DWI and MRS for the non-invasive characterization of brain tumors. The combined protocol achieved a high diagnostic accuracy of 86%, providing crucial physiological and metabolic data that is unattainable with conventional imaging alone. Our findings align with and build upon a growing body of evidence advocating for the use of these advanced sequences in routine neuro-oncology protocols [10,11].

A central finding of this study is the inverse correlation between tumoral ADC values and tumor grade, supporting the principle that ADC serves as a surrogate marker for cellularity. Our results show a clear spectrum, with highly cellular malignant tumors like Lymphoma (ADC=0.50 x 10^{-3} mm^2/s) and Metastasis (ADC=0.64 x $10^{-3}mm^2/s$) exhibiting the lowest ADC values, while benign, less-cellular lesions like Pilocytic Astrocytoma (ADC=1.50 x 10^{-3} mm^2/s) showed the highest. This is consistent with prior work. Our ROC analysis identified an ADC cut-off of 0.85 x 10^{-3} mm^2/s as the optimal threshold for malignancy, yielding a high sensitivity of 94%. This confirms DWI as an excellent initial tool for raising suspicion of malignancy. However, the 75% specificity of ADC underscores its limitations. We observed an overlap in ADC values, particularly between high-grade gliomas and some benign lesions like meningiomas (mean ADC 0.85 x 10^{-3} mm^2/s). This is where the metabolic data from MRS becomes essential.

The most robust finding of our study was the superior diagnostic performance of the **Cho/Cr ratio**. It emerged as the best single differentiator of benign and malignant lesions, with an AUC of 0.932 and a high specificity of 86.7% at a cut-off of 1.72. This demonstrates that the marker of cell proliferation (Cho) is a more specific indicator of malignancy than the marker of cellular density (ADC). These findings are strongly supported by the literature; multiple studies have identified the Cho/Cr and Cho/NAA ratios as reliable indicators of tumor grade. Our results reinforce this, showing a dramatic elevation in Cho/Cr for Metastasis (4.10), Lymphoma (3.30), and GBM (2.50), in stark contrast to benign lesions. Interestingly, the Cho/NAA ratio, while still significant, was a less effective differentiator (AUC 0.710) in our cohort. This may be due to the variable reduction of NAA across different tumor types, making it a less stable denominator than Cr.

The presence of lipid peaks also proved to be a highly specific, albeit less sensitive, marker for high-grade malignancy and necrosis. Its presence in 100% of lymphomas and 80% of GBMs, but absence in all Pilocytic Astrocytomas,

Neuroblastomas, and Oligodendrogliomas, aligns with findings from Yamasaki et al. (2005) and points to its utility as a "red flag" for aggressive pathology.

Furthermore, this study highlights an advanced application: the use of peritumoral ADC values to differentiate infiltrative from circumscribed lesions. We found a significantly higher peritumoral ADC in gliomas compared to metastases. This reflects a key pathophysiological difference: the high ADC in the peritumoral region of a glioma (1.80×10^{-3} mm^2/s) represents tumor cell infiltration, while the lower ADC around a metastasis (1.36×10^{-3} mm^2/s) represents vasogenic edema. This finding has direct clinical implications, helping to distinguish a high-grade glioma from a solitary metastasis, a common and critical diagnostic dilemma [13].

Implications, Limitations, and Future Research

Clinical Implications

The findings of this study have direct clinical implications. The combined use of DWI and MRS can significantly enhance diagnostic certainty in the pre-operative setting. This non-invasive characterization can help differentiate challenging cases (e.g., lymphoma vs. glioblastoma vs. metastasis) and guide neurosurgical planning. For example, identifying a lesion with a very low ADC and high Cho/Cr (suggestive of lymphoma) may prompt a biopsy rather than a large resection. Conversely, identifying infiltrative patterns via peritumoral ADC can help surgeons plan a wider resection margin for a glioma.

LIMITATIONS

This study has several limitations :

- **Small Sample Size:** A cohort of 50 patients limits the statistical power for sub-group analysis of less common tumor types.
- **Single-Center Study:** As a non-randomized study at a single teaching hospital, selection bias cannot be fully excluded.
- **Technical Variability:** MRS voxel placement is operator-dependent. While efforts were made to standardize placement, minor variations in positioning could influence metabolite ratios.
- **Parameter Overlap:** Despite statistically significant differences, there remains an overlap in ADC and metabolite values between tumor grades, meaning no single metric is 100% definitive.

Future Research

As concluded in the initial study, further research with a larger, multi-center sample size is warranted. This would help to better define the specific cut-off values for ADC and metabolite ratios for a wider variety of brain tumors. Future studies should also aim to standardize imaging protocols across institutions to promote wider clinical adoption and explore the use of machine learning algorithms to integrate these complex datasets for even more accurate, automated tumor classification.

CONCLUSION

This study demonstrates that the combination of Diffusion-Weighted MRI and Magnetic Resonance Spectroscopy is a reliable and accurate non-invasive method for differentiating benign and malignant brain tumors, achieving a diagnostic accuracy of 86% against the gold standard of histopathology.

The key findings are :

1. The **Cho/Cr ratio** is the single most powerful biomarker, with a cut-off of 1.72 yielding 94.3% sensitivity and 86.7% specificity (AUC 0.932).
2. The tumoral **ADC value** is an excellent marker for cellularity, with a cut-off of 0.85 providing 94% sensitivity.
3. The presence of a **Lipid peak** is a highly specific indicator of high-grade malignancy and necrosis.
4. **Peritumoral ADC** analysis can help differentiate infiltrative gliomas from circumscribed metastases.

The integration of this functional and metabolic data into standard imaging protocols enhances diagnostic confidence, improves the differentiation of brain masses, and provides invaluable information for neurosurgeons in pre-operative planning and patient management.

REFERENCES

1. Svolos, P.; Kousi, E.; Kapsalaki, E.; Theodorou, K.; Fezoulidis, I.; Kappas, C.; Tsougos, I. The role of diffusion and perfusion weighted imaging in the differential diagnosis of cerebral tumors: A review and future perspectives. *Cancer Imaging* 2014, 14, 20.
2. Romano, A.; Bozzao, A.; Bonamini, M.; Fasoli, F.; Ferrante, M.; Floris, R.; Colonnese, C.; Fantozzi, L.M. Diffusion-weighted MR Imaging: Clinical applications in neuroradiology. *Radiol. Med.* 2003, 106, 521-548.
3. Murakami, R.; Sugahara, T.; Nakamura, H.; Hirai, T.; Kitajima, M.; Hayashida, Y.; Baba, Y.; Oya, N.; Kuratsu, J.; Yamashita, Y. Malignant supratentorial astrocytoma treated with postoperative radiation therapy: Prognostic value of pretreatment quantitative diffusion-weighted MR imaging. *Radiology* 2007, 243, 493-499.

4. Yamasaki, F.; Kurisu, K.; Satoh, K.; Arita, K.; Sugiyama, K.; Ohtaki, M.; Takaba, J.; Tominaga, A.; Hanaya, R.; Yoshioka, H.; et al. Apparent diffusion coefficient of human brain tumors at MR imaging. *Radiology* 2005, 235, 985-991.
5. Barker PB. N-acetyl aspartate--a neuronal marker? *Ann Neurol.* 2001;49(4):423-424.
6. Gupta RK, Cloughesy TF, Sinha U, et al. Relationships between choline magnetic resonance spectroscopy, apparent diffusion coefficient and quantitative histopathology in human glioma. *J Neurooncol.* 2000;50(3):215-226.
7. Dasgupta A, Gupta T, Jalali R. Indian data on central nervous tumors: A summary of published work. *South Asian J Cancer.* 2016 Jul-Sep;5(3): 147-53.
8. De Graaf, R.A. (2007). *In-vivo NMR Spectroscopy: Principles and Techniques* (Chichester, UK: John Wiley & Sons).
9. Yamasaki F, Takaba J, Ohtaki M, Abe N, Kajiwara Y, Saito T, Yoshioka H, Hama S, Akimitsu T, Sugiyama K, Arita K, Kurisu K. Detection and differentiation of lactate and lipids by single-voxel proton MR spectroscopy. *Neurosurg Rev.* 2005 Oct;28(4):267-77.
10. S., S. P., & Kattoju, S. Role of magnetic resonance spectroscopy and diffusion-weighted imaging in characterizing intra axial brain tumours. *International Journal of Research in Medical Sciences* 2023; 11(10): 3722-3728.
11. Romano A, Palizzi S, Romano A, Moltoni G, Di Napoli A, Maccioni F, Bozzao A. Diffusion Weighted Imaging in Neuro-Oncology: Diagnosis, Post-Treatment Changes, and Advanced Sequences-An Updated Review. *Cancers (Basel).* 2023 Jan 19;15(3):618.
12. Ankush A, Sardessai S. Role of MRSI Major Metabolite Ratios in Differentiating Between Intracerebral Ring-Enhancing Neoplastic and Non-Neoplastic Lesions, High-Grade Gliomas and Metastases, and High-Grade and Low-Grade Gliomas. *Cureus.* 2022 Nov 23;14(11):e31841.
13. Würtemberger U, Rau A, Diebold M, Becker L, Hohenhaus M, Beck J, Reinacher PC, Erny D, Reisert M, Urbach H, Demerath T. Advanced diffusion MRI provides evidence for altered axonal microstructure and gradual peritumoral infiltration in GBM in comparison to brain metastases. *Clin Neuroradiol.* 2024 Apr 29.
14. Aydın ZB, Aydın H, Birgi E, Hekimoğlu B. Diagnostic Value of Diffusion-weighted Magnetic Resonance (MR) Imaging, MR Perfusion, and MR Spectroscopy in Addition to Conventional MR Imaging in Intracranial Space-occupying Lesions. *Cureus.* 2019 Dec 18;11(12):e6409.
15. Zeng Q, Liu H, Zhang K, Li C, Zhou G. Non-invasive evaluation of cerebral glioma grade by using multivoxel 3D proton MR spectroscopy. *Magn Reson Imaging.* 2011 Jan;29(1):25-31.